ACS APPLIED MATERIALS & INTERFACES

Research Article

www.acsami.org

Surface Oxide Effect on Optical Sensing and Photoelectric Conversion of α-In_2Se_3 Hexagonal Microplates

Ching-Hwa Ho,*[,†,‡] Chien-Hao Lin,[‡] Yi-Ping Wang,[‡] Ying-Cen Chen,[†] Shin-Hong Chen,[†] and Ying-Sheng Huang[‡]

[†]Graduate Institute of Applied Science and Technology and [‡]Department of Electronic Engineering, National Taiwan University of Science and Technology, Taipei 106, Taiwan, Republic of China

ABSTRACT: The surface formation oxide assists of visible to ultraviolet photoelectric conversion in α-In_2Se_3 hexagonal microplates has been explored. Hexagonal α-In_2Se_3 microplates with the sizes of 10s to 100s of micrometers were synthesized and prepared by the chemical vapor transport method using ICl_3 as a transport agent. Many vacancies and surface imperfection states have been found in the bulk and on the surface of the microplate because of the intrinsic defect nature of α-In_2Se_3. To discover physical and chemical properties and finding technological uses of α-In_2Se_3, several experiments including transmission electron miscopy (TEM), X-ray photoelectron spectroscopy (XPS), surface photovoltage (SPV), photoluminescence (PL), surface photoresponse (SPR), photoconductivity (PC), and thermoreflectance (TR) measurements have been carried out. Experimental results of TEM, XPS, SPV, PL, and SPR measurements show that a surface oxidation layer α-$In_2Se_{3-3x}O_{3x}$ ($0 \le x \le 1$) has formed on the crystal face of α-In_2Se_3 in environmental air with the inner layer content close to In_2Se_3 but the outermost layer content approaching In_2O_3. The near band edge transitions of α-In_2Se_3 microplates have been probed experimentally by TR and PC measurements. The direct band gap of α-In_2Se_3 has been determined to be 1.453 eV. The SPV result shows a maximum quantum efficiency of the surface oxide α-$In_2Se_{3-3x}O_{3x}$ ($0 \le x \le 1$) that presents a peak photoresponse near 2.18 eV. The analyses of SPV, SPR, PL, TR, and PC measurements revealed that the surface oxide layer facilitates the conversion of the ultraviolet to the visible range while the native defects (Se and In vacancies) sustain photoconductivity in the near-infrared region. On the basis of the experimental results a wide-energy-range photodetector that combines PC- and SPR-mode operations for α-In_2Se_3 microplate has been made. The testing results show a well-behaved function of photoelectric conversion in the near-infrared to ultraviolet region via the auxiliary forming of surface oxide on the crystalline face of the α-In_2Se_3 microplates.

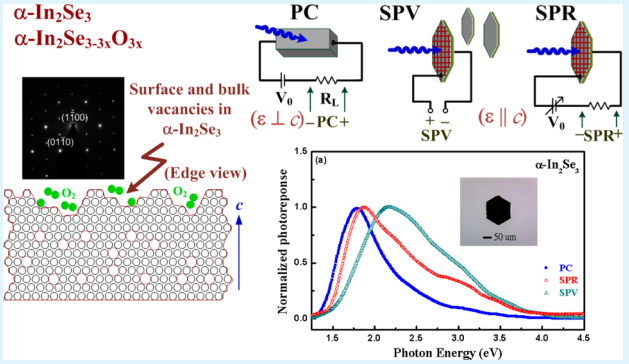

KEYWORDS: *III−VI compound, In_2Se_3, surface oxidation, photoelectric conversion, surface photovoltage, photodetector*

INTRODUCTION

Indium selenide (α-In_2Se_3) is one of the most important narrow-gap materials suitable for solar energy conversion and optoelectronics applications. The potential uses of indium selenide are as solar-cell material,[1,2] field-effect transistor,[3,4] phase-changed memory,[5,6] logic device,[7] anisotropic photoconductivity device,[8,9] visible-light photodetector,[10,11] and lithium ion batteries.[12] Owing to the mismatch of valence electron numbers (i.e., In^{III} and Se^{VI}), In−Se compounds often show a variety of valency-changed structures with different stoichiometry and crystalline phases. The generally found stoichiometries for indium selenides are InSe,[13] In_6Se_7,[14] and In_2Se_3.[15−17] These selenides possess miscellaneous crystal structures, dissimilar band diagrams as well as different band gaps. Even for the In_2Se_3 compound, it is interesting that the alloy possesses at least four different crystalline phases denoted as α, β, γ, δ, and κ found in the literature.[18−21] However, the most popular and well studied modifications of In_2Se_3 include α, β, and γ phases. The crystalline form of these phases is a layered structure with different arrangement of In and Se atoms connected in one monolayer along the c axis.[16] The main difference of the connection chain consists of Se−In−Se−In−Se tetrahedral configuration or Se−In−Se═In═Se tetra-octahedral configuration, where "−" and "=" are the chemical bonds in tetrahedral and octahedral coordinations.[17] The reported values of lattice constants for the layered In_2Se_3 are a = 4.025 Å and c = 19.235 Å for α-In_2Se_3, a = 4.000 Å and c = 28.33 Å for β-In_2Se_3, and a = 7.1286 Å and c = 19.382 Å for γ-In_2Se_3, respectively.[18] The main discrepancy between the α and β phases is the dissimilarity in c axis while the major difference between the α and γ phases is the length change of a axis.

α-In_2Se_3 is the most stable phase of indium selenide with hexagonal layer structure stacking in the Se−In−Se═In═Se tetra-octahedral configuration. The calculated band gap of α-

Received: January 18, 2013
Accepted: March 2, 2013
Published: March 2, 2013

In_2Se_3 is around 1.48 eV.[17] Because of the misvalency between III and VI atoms, a natural defect-like phase of $\square_1$-III_2−VI_3 is usually found in the unit cell of general α-In_2Se_3 layers. The "$\square$" is a vacant site (vacancy) of Se or In atom. Owing to the In_2Se_3 originally showing n-type semiconducting behavior,[5] the indium selenide is inferred to have stronger Se-vacancy effect (donor) in building the unit cell. The Se vacancies may dominate the band edge and transport property of the layer compound. By the existence of dangling bonds of the Se vacancies, a surface oxidation layer can easily form on the material interface of α-In_2Se_3 under ambient air. This situation is similar to its chalcogenide counterpart In_2S_3 for which there exists one $In_2S_{3-3x}O_{3x}$ layer on its crystal surface.[22,23] Indium chalcogenides are generally the solar energy materials with lower band gap (e.g., E_g < 1.5 eV for α-In_2Se_3 and E_g = 1.935 eV for In_2S_3).[24] The existing $In_2S_{3-3x}O_{3x}$ oxide layer on the surface of In_2S_3 can assist photoelectric conversion of sunlight ranging from 2 eV to the energies larger than 3.2 eV.[25] The α-In_2Se_3 is even better for energy conversion because its direct band gap is close to the optimal value of 1 eV as compared with that of In_2S_3. The surface oxide layer on In_2Se_3 may also contribute to the photoelectric conversion in the higher energy region. However, to date, all the researches are focused on studying the intrinsic In_2Se_3 property and very rarely on studying the surface formation oxide (e.g., $In_2Se_{3-3x}O_{3x}$ from environment) which can improve photoelectric conversion properties of the indium selenide.

In this paper, surface oxide and bulk characteristics of α-In_2Se_3 microplates have been evaluated by transmission electron miscroscopy (TEM), X-ray diffraction, X-ray photoelectron spectroscopy (XPS), surface photovoltage (SPV), photoluminescence (PL), surface photoresponse (SPR), photoconductivity (PC), and thermoreflectance (TR) measurements. The direct band gap of α-In_2Se_3 was determined to be ∼1.453 eV by TR. The experimental analyses of X-ray diffraction, XPS, SPV, SPR, PL, and PC show that the lower-gap α-In_2Se_3 has a superior photoresponse near short-wavelength region because of the formation of stoichiometric surface oxide α-$In_2Se_{3-3x}O_{3x}$ on the outer layer of the α-In_2Se_3 microplates. The PL spectra show that the outermost layer of the surface oxide (α-$In_2Se_{3-3x}O_{3x}$) is approximately close to that of In_2O_3, which emits blue to ultraviolet luminescence. Spectral photoelectric-conversion efficiency of α-In_2Se_3 also shows an increase from 2 to 4 eV (evident by SPV) because of the existence of surface oxide on the α-In_2Se_3. PC and SPR measurements show that the bulk α-In_2Se_3 dominates an absorption range of near-infrared to visible while the surface oxide α-$In_2Se_{3-3x}O_{3x}$ handles photoelectric conversion from the visible to the ultraviolet portion. The sunlight spectrum of near-infrared, visible, and ultraviolet can be efficiently absorbed to achieve photoelectric conversion in the surface oxide assisted α-In_2Se_3 hexagonal microplates.

EXPERIMENTAL SECTION

Preparation of α-In_2Se_3 Microplates. The microcrystals of α-In_2Se_3 with various sizes of tens to thousands μm^2 were grown by the chemical vapor transport method using ICl_3 as a transport agent. Prior to the crystal growth, the pure elements of In (purity 99.9999%) and Se (purity 99.999%) with stoichiometry together with a small amount of transport agent (∼ 5 mg/cm^3) were put into a quartz ampule (outer diameter 22 mm, inner diameter 17 mm, and length 20 cm), which was then cooled with liquid nitrogen, evaluated to ∼10^{-6} Torr and sealed. The mixture was slowly heated to 800 °C and kept at this temperature for two days for synthesis. The slow heating process is necessary for preventing explosions in the ampule because of the strongly exothermic reaction between the elements. For crystal growth of the micro plates, the growth temperature was set as 950 °C (heating zone) → 800 °C (growth zone) with a gradient of −7.5 °C/cm. The reaction was kept for 10 days. After the growth, synthetic In_2Se_3 micro plates have a hexagonal shape. The size of the areas are from ten to 100s μm^2 and some of them are higher up to several mm^2. The as-grown microplates show a black and shiny surface. The thickness of the microplates ranges from 10s to 100s μm. The weak van der Waals bonding between the layers means that the microplate can be easily separated to thin out from the c plane by using a razor blade or a Scotch tape. The results of X-ray diffraction and TEM confirm an α crystalline phase of the as-grown In_2Se_3 microplates. The lattice constants of the as-grown α-In_2Se_3 are determined to be a = 4.018 Å and c = 19.228 Å, respectively.

Characterization. XPS measurements were implemented by a Scientific K-Alpha system with a monochromatic Al K_α line source. The X-ray spot size in the system can be adjusted to 15−400 μm and the energy resolution can reach ∼0.02 eV. The experiments were done on the as-grown c plane of the chalcogenide in an analysis chamber with an ultimate vacuum reaching 10^{-9} mbar. An argon ion source facilitates the dry etching process of the sample.

TR experiments of the α-In_2Se_3 layers were implemented using an indirect heating method with a gold-evaporated quartz plate as the heating element.[26,27] The thin layered sample was closely attached on the heating element by silicone grease. The on−off heating disturbance uniformly modulates the α-In_2Se_3 microplate periodically. The incident and reflected lights can be guided by a silica fiber. An 150 W tungsten halogen lamp (or an 150 W xenon-arc lamp) filtered by a PTI 0.2-m monochromator provided the monochromatic light. The incident light is focused onto the sample with a spot size less than 100 μm^2. An EG&G type HUV-2000B Si photodetector acted as the detection unit, and the TR signal was measured and recorded via an EG&G model 7265 lock-in amplifier. PL experiments were carried out using a QE65000 spectrometer. A closed-cycle cryogenic refrigerator with a thermometer controller facilitates the low-temperature measurements for PL and TR measurements.

The SPV, SPR, and PC experiments are the optical techniques that do not need any optical sensor. The photodetector is the sample itself. The measurement configurations of the SPV, SPR, and PC techniques can be referred to Figure 3b. For SPV and SPR measurements, a thin α-In_2Se_3 microplate is attached on a copper sample holder by silver paste, the holder acts as the bottom electrode of the measurements. The top surface of small area sample can be micropatterened and coated with one golden or copper mesh on the sample plane. This is the top electrode of SPV and SPR measurements. The incident monochromatic light source of SPV and SPR is similar to TR. For SPV measurements, the photoexcited electron−hole pairs from the surface band-bending region were extracted out from the top and bottom electrodes of the capacitor-like configuration, and then sent to a low-noise amplifier. The incident light was chopped at 20 Hz, and the photoelectric conversion response (from the low-noise amplifier) of α-In_2Se_3 was recorded via an EG&G model 7265 lock-in amplifier. For SPR measurements, an electric field was applied perpendicular to the c plane of α-In_2Se_3 between the top and the bottom electrodes. It is similar to the electric-field operation of a thin-film solar cell. A load resistor connected in series with the sample was used for sensing the photocurrent under the light's illumination. A DC voltage was supplied to the circuit. For PC measurements, the α-In_2Se_3 sample was cut into a rectangular shape with the indium coated two ends acting as the ohmic contact electrodes. The main difference between SPR and traditional PC measurements is the direction that the electric field is applied to the sample. The SPR is normal to the c plane ($\varepsilon \| c$-axis) while PC is the in-plane photoconductivity of the c plane ($\varepsilon \perp c$-axis) of the α-In_2Se_3 microplates. Specially, SPV and SPR measurements are sensitive for the detection of the photoelectric conversion response from the surface oxide existing on the α-In_2Se_3 microplate. All the measured PC, SPV, and SPR spectral photoresponses are calibrated using a broadband thermal sensor with a measurement range from 1.25 to 5 eV.

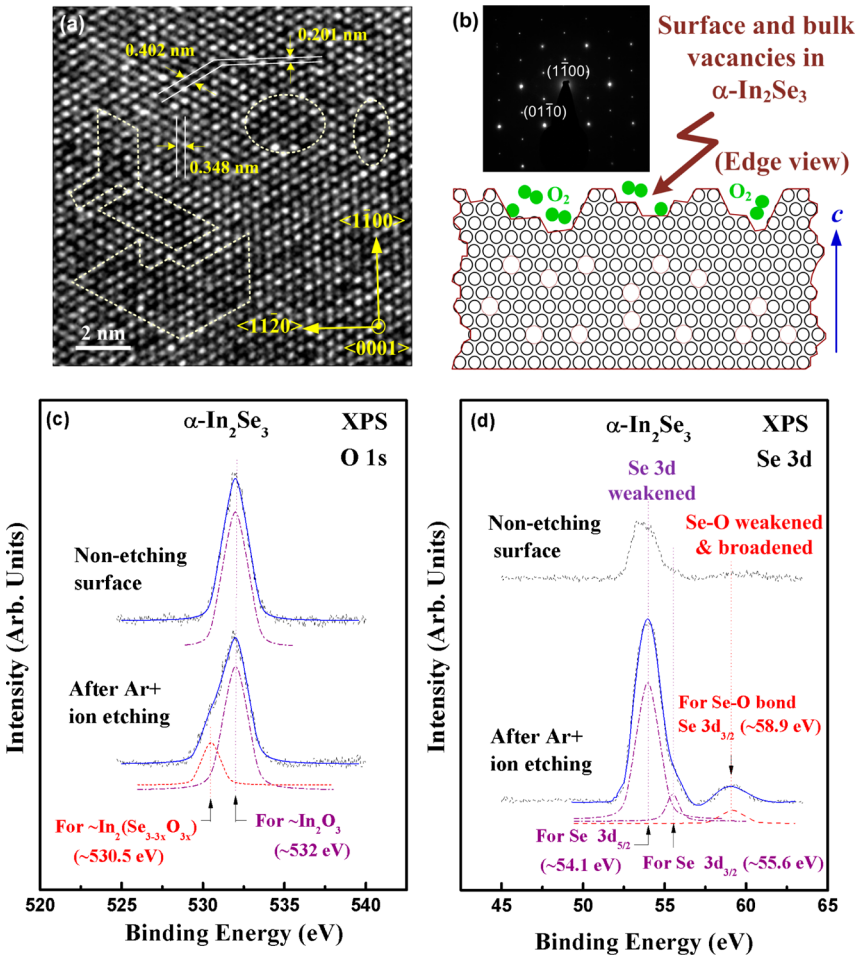

Figure 1. (a) HRTEM image of the *c* plane of α-In_2Se_3 after Ar^+ ion etching. Some enclosed regions show lack of top layer atoms. (b) The selected-area electron diffraction pattern of the *c*-plane α-In_2Se_3. The representative scheme for surface and bulk vacancies in α-In_2Se_3 (edge view) is also shown. (c) The XPS spectra of oxygen 1s orbital with nonetching face and etched surface for α-In_2Se_3. (d) Se 3d state for a nonetching and a surface-etched α-In_2Se_3.

RESULTS AND DISCUSSION

Figure 1a shows the high-resolution transmission electron microscopy (HRTEM) image of the *c*-plane α-In_2Se_3 microplate after Ar^+ ion etching for 30 s. The selected-area electron diffraction pattern shown in the upper part of Figure 1b verifies that the TEM image in Figure 1a is a *c*-plane α-In_2Se_3. Because of the defect nature by misvalency of III and VI (In_2Se_3), the Se vacancies can react (replace) with environmental oxygen to form a surface oxidation state on the crystal face of indium selenide. This situation can be discovered from the surface-etched In_2Se_3 in Figure 1a for many enclosed regions are missing with the top-layer atoms (i.e., marked with dashed-lines areas) on the *c* plane. According to the HRTEM image shown in Figure 1a, the lattice constant of *a*-axis for In_2Se_3 can be determined to be ~0.402 nm, which matches well with the α-phase indium selenide.[1,28] The representative scheme for showing the vacant-sites structure of α-In_2Se_3 microplate near surface and into bulk (edge view) is depicted in the lower part of Figure 1b. When the as-grown α-In_2Se_3 microplate was put in air, the surface and bulk vacancies of In_2Se_3 may have the possibility to react with ambient oxygen, specially on the surface. The surface reaction resembles that of gas sensing in materials by first adsorption with O_2. The interaction with atmospheric oxygen can produce ionosorption of molecular O_2^{4-} and atomic (O^{2-}, O_2) species at reaction temperatures of 25−500 °C.[29] At room temperature, nearly all of the adsorbed atmospheric oxygen by vacancies of In_2Se_3 will be O_2^{4-}. The reaction kinetics for the oxygen adsorption and charge transfer can be described as follows:

$$O_2(\text{gas}) \leftrightarrows O_2(\text{ads})$$
$$O_2(\text{ads}) + 4e^- \leftrightarrows O_2^{4-} \quad (1)$$

.

However, the charge transfer and chemical reaction between the occupants O_2^{4-} (that stay in the Se−Se vacancies) and the cation In^{3+} ions by taking into account the stoichiometric change from inner layer to outermost layer will become:

$$2\cdot In_2Se_{(3-3x\cdot\square)} + 3\cdot x\cdot O_2^{4-} \leftrightarrows 2\cdot In_2Se_{3-3x}O_{3x}$$
$$(0 \le x \le 1) \quad (2)$$

,where the oxygen content is changed from $x = 0$ (the inner layer ~In_2Se_3) to $x = 1$ (the outermost layer ~In_2O_3), and "□" is the selenium vacancy in the unit cell of α-In_2Se_3. To verify the result of forming the surface oxide on the α-In_2Se_3, XPS measurements were carried out at 300 K. Figure 1c shows the XPS spectra of the oxygen 1s orbital (dashed lines) for a nonetching face of as-grown α-In_2Se_3 as well as for the *c* plane of indium selenide after Ar^+ ion etching for 30 s. The spectral

dx.doi.org/10.1021/am400128e | ACS Appl. Mater. Interfaces 2013, 5, 2269−2277

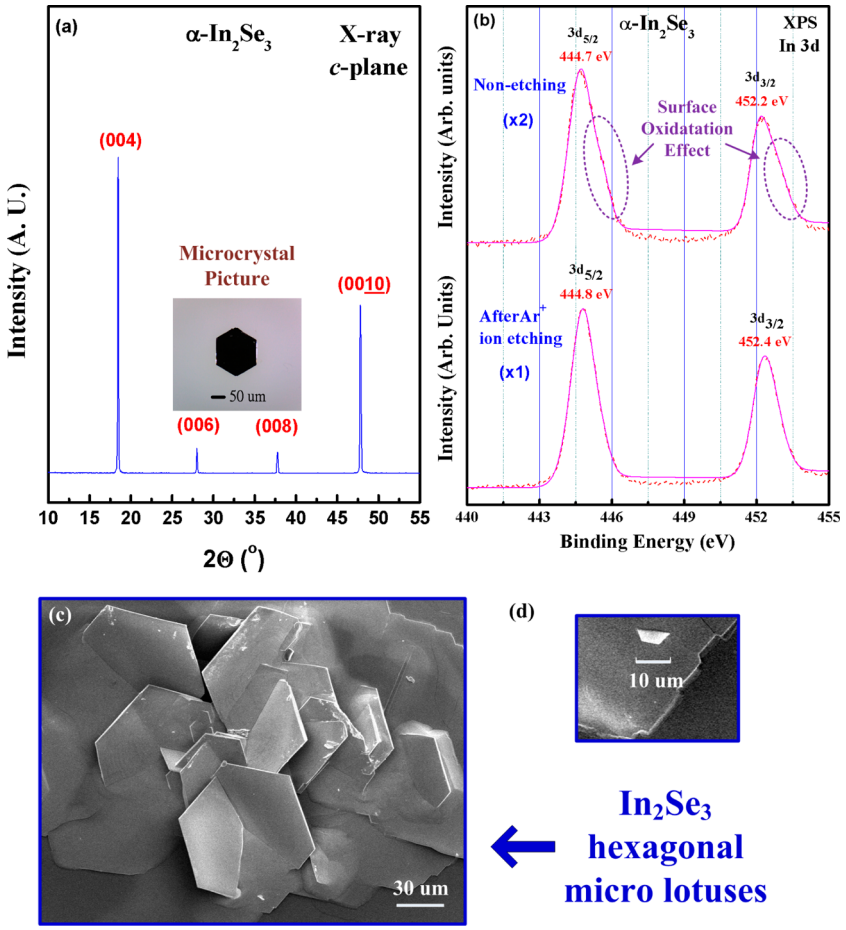

Figure 2. (a) *c*-Plane X-ray diffraction pattern of α-In_2Se_3 crystal with higher order peaks. A microcrystal image for the α-In_2Se_3 hexagonal microplate is also shown in the inset. (b) The In 3d XPS spectra of a nonetching and a surface-etched α-In_2Se_3. (c) The as-grown α-In_2Se_3 hexagonal microplates crowding together to form a beautiful cluster as "hexagonal micro lotuses". (d) The minimum length of a hexagonal microplate is about 10 μm.

analysis using a Lorentzian-function fit reveals that only one XPS peak located at ~532 eV can be observed for the nonetching surface of α-In_2Se_3, and the energy position matches well with the O 1s orbital of In_2O_3 (i.e., 532.1 eV).[30] For the surface-etched α-In_2Se_3 shown in the lower part of Figure 1c, an additional peak is detected at ~530.5 eV which corresponds to the energy position coming from In(OX).[31] The oxygen deficient In(OX) signal may come from the surface oxidation state $In_2Se_{3-3x}O_{3x}$. The surface-etched sample in Figure 1c also shows a weakened XPS peak of O 1s related to that of indium oxide centered at ~532 eV. To further verify that the $In_2Se_{3-3x}O_{3x}$ layer was formed in between the In_2Se_3 and the outermost In_2O_3 layer, XPS measurements of Se 3d orbital for a surface-etched and a nonetching α-In_2Se_3 microplate are respectively carried out. The results are shown in Figure 1d. Two XPS peaks at ~54.1 eV and ~55.6 eV which correspond to the Se $3d_{5/2}$ and Se $3d_{3/2}$ electrons for the α-In_2Se_3 microplate are clearly detected in the surface-etched sample.[32] Specially, one additional peak at ~58.9 eV appears [see the lower part of Figure 1d]. This electronic state may be attributed to the Se $3d_{3/2}$ orbital caused by the Se−O bond. The energy position of 58.9 eV is similar to a bonding energy of 58.6 eV for the Se−O bond detected in SeO_2.[33] For the nonetching surface of α-In_2Se_3 [see the upper part of Figure 1d], the Se 3d peaks show weakening, and the Se−O bond signal is also weakened and broadened owing to the relatively very low Se content existingd on the surface of the α-In_2Se_3 microplate. The XPS results in Figures 1c and 1d verify the formation of surface oxide layer $In_2Se_{3-3x}O_{3x}$ $(0 \leq x \leq 1)$ on the crystal plane of α-In_2Se_3 with lower oxygen content constructing the inner part but higher oxygen content forming the outermost layer.

Displayed in the inset of Figure 2a is the microplate picture of α-In_2Se_3 of hexagonal shape with a width of ~100 μm. The α-phase diindium triselenide is a hexagonal layer-type structure with weak van der Waals bonding existing in between the monolayers (i.e., stacking along *c*-axis). The pronounced outline of the microplate is a distinctly hexagonal *c* plane. As shown in Figure 2a, the single crystal X-ray diffraction pattern displays only one *c*-plane peak and its higher-order interplannar spacings for the α-In_2Se_3. The peak pattern provides the information about lattice constant *c*, which was determined to be $c \approx 19.228$ Å. Figure 2b shows a doublet of XPS peak structures of In 3d for a surface-etched and a nonetching α-In_2Se_3 microplate. The fitted bonding energies of In $3d_{5/2}$ and In $3d_{3/2}$ for the surface-etched α-In_2Se_3 are determined to be ~444.8 eV and ~452.4 eV, respectively. The energy values are close to previous XPS results detected by In_2Se_3.[31] For the nonetching α-In_2Se_3 [see the upper part of Figure 2b], the peak features of In $3d_{5/2}$ and In $3d_{3/2}$ show a broadened line-width and a weakened intensity owing to the stronger surface oxidation effect on the microplate. The nonetching α-In_2Se_3 also shows slight red shift of binding energies of In $3d_{5/2}$

(~444.7 eV) and In $3d_{3/2}$ (~452.2 eV) with respect to those of the surface-etched α-In_2Se_3 shown in Figure 2b. All the XPS results in Figures 1 and 2 confirm that a surface oxidation layer may form on the crystal face of the α-In_2Se_3 microplate. This phenomenon is maybe a general characteristic for an indium chalcogenide with a defect nature.[22] When growing the α-In_2Se_3 hexagonal microplates using chemical vapor transport, the growth kinetics of chemical vapor transport with the assistance of a transport agent can be described as follows:

$$i\cdot A_{(s)} + j\cdot B_{(g)} \leftrightarrows k\cdot C_{(g)} \quad (3)$$

,where A is the synthesized material, B is the transport agent, and C is the gaseous synthesized compound (A, C = In_2Se_3 and B = ICl_3). The formation of α-In_2Se_3 microplates must proceed by the reversed reaction of eq 3 by growing the microplate crystals at the cool end of the quartz ampule with temperature profile setting as 950 → 800 °C (i.e., gradient −7.5 °C/cm). The easily forming face of α-In_2Se_3 can be the c plane. It means that the slowest growth rate of the hexagonal α-In_2Se_3 is along c axis, and an approximately equal-fast growth rate will occur on the individual edge plane of the hex-octahedron to appear in a nearly identical edge length. With this rule, the α-In_2Se_3 microcrystal can easily form a perfect hexagon microplate as shown in the inset of Figure 2a. The scanning electron microscopy (SEM) image of Figure 2c displays different sizes of hexagonal microplates which can crowd together to form some well-defined hexagonal micro lotuses for the α-In_2Se_3. The minimum size (length) of the α-In_2Se_3 hexagonal microplate is about 10 μm which can be evident in the SEM picture of Figure 2d. A hexagonal microplate with a length size larger than 100 μm is used for optical studies. The shape is similar to the microplate shown in the inset of Figure 2a.

Figure 3a shows the normalized SPV, SPR, and PC spectra of the α-In_2Se_3 hexagonal microplate by using a tungsten halogen lamp in the energy range of 1.25 to 4.5 eV. The photoresponsivities of SPV, SPR, and PC are normalized to maximum peak intensities of each spectrum for comparing the energy position of each peak photoresponse. The maximum peak photoresponses of the spectra are marked with SPV P1, SPR P1, and PC P1, respectively. As shown in Figure 3a, the energy position of PC P1 is about 1.77 eV, which is lower than that of ~1.89 eV for SPR P1 and that of ~2.18 eV for SPV P1. Figures 3b and 3c show, respectively, the measurement arrangements and band configurations of PC, SPV, and SPR experiments. For the PC measurement, the sample was cut into a rectangular shape with an electric field ε applied in the $\varepsilon \perp c$ direction. The PC photoresponse was derived from a load resistor R_L. The values of applied voltage V_0 and load resistor R_L are 25 V and 10 MΩ, respectively. The α-In_2Se_3 hexagonal microplate has generally a surface oxide forming on the bulk crystal plane. Because In_2O_3 has a larger band gap (>3.2 eV)[33,34] than In_2Se_3 (<1.5 eV), the $In_2Se_{3-3x}O_{3x}$ ($0 \le x \le 1$) oxide forming on the α-In_2Se_3 can be approximately regarded as two parallel resistors [R_{ox} and R_s as indicated in Figure 3c] with a lower value of R_s (for In_2Se_3) and higher resistance of R_{ox} (for surface oxide) because of their different band gaps. The measured photoresponses of PC may be inferred to mainly come from the bulk α-In_2Se_3, not from the surface oxide with larger band gap. This is why the energy position of PC P1 in Figure 3a is lower than those of SPR P1 and SPV P1 because the contribution of PC is largely from the lower band gap of α-In_2Se_3. For SPV and SPR measurements, the surface electric field ε is parallel to the c-axis ($\varepsilon \| c$). The top electrode (i.e., copper mesh) contacts the crystal surface of the α-In_2Se_3 microplate while the bottom electrode is a copper holder. It is expected to have high photoelectric-conversion responses coming from the surface oxide with SPV and SPR measurements. As shown in the normalized SPR and SPV spectra of Figure 3a, the surface oxide contributes higher photoelectric conversion responses than that of the PC spectrum, and their energy positions (SPR P1 and SPV P1) are larger than that of PC P1. Specially, the SPV photoresponse spectrum demonstrates the real photoelectric conversion responses via the assistance of the surface band-bending effect just like a junction solar cell. The representative band diagram for the heterojunction layers of In_2O_3, $In_2Se_{3-3x}O_{3x}$, and In_2Se_3 for the SPV configuration is depicted in the middle part of Figure 3c. Because the energy position of SPV P1 is higher than those of SPR P1 and PC P1, the photoelectric conversion response of the SPV mode is hence inferred to come mostly from $In_2Se_{3-3x}O_{3x}$ and In_2O_3 but less from the α-In_2Se_3. The quantum efficiency of the α-In_2Se_3 hexagonal microplate with the SPV mode operation can be evaluated from the measured photoresponse described as

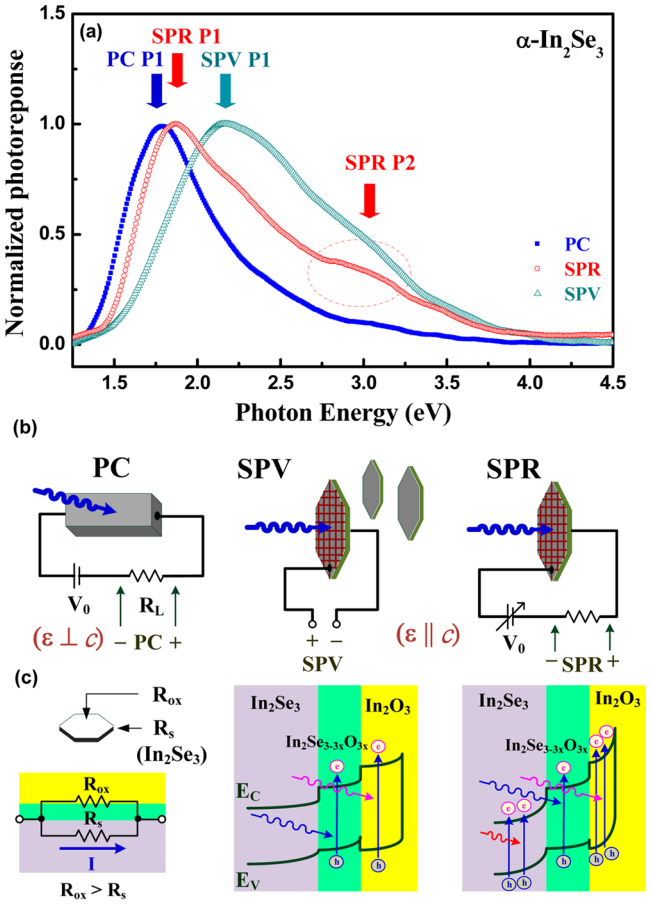

Figure 3. (a) Normalized PC, SPV, and SPR photoresponse spectra of α-In_2Se_3 at room temperature. (b) Measurement arrangements of PC, SPV, and SPR experiments. (c) The equivalent circuit and heterojunction band-bending diagrams for the α-In_2Se_3 hexagonal microplate under PC, SPV, and SPR mode operations.

$$\eta = R\cdot(h\nu/q) \quad (4)$$

,where η is quantum efficiency, R represents the measured photoresponsiveness, $h\nu$ refers to photon energy (in eV), and q denotes the electron charge. It also means that quantum

dx.doi.org/10.1021/am400128e | ACS Appl. Mater. Interfaces 2013, 5, 2269−2277

efficiency is the ratio of numbers for generated charge carrier to that of incident photon at a certain wavelength. As shown in Figure 3a, the peak photoresponse of the SPV spectrum is around 2.18 eV. The real (i.e., un-normalized) photoresponse of SPV at 2.18 eV is $R = 2.01 \times 10^{-2}$ A/W. The value of the photoresponse leads a calculated quantum efficiency of $\eta \approx 4.36\%$ near the peak response close to 2.18 eV using eq 4. The peak energy value approaches the green portion near the maximum responsivity of sunlight on earth. The SPV photoresponse in Figure 3a covers largely from the visible to the ultraviolet region in contrast to that of the PC spectrum which dominates mainly in the near-infrared region. This result confirms that the surface oxide $In_2Se_{3-3x}O_{3x}$ strongly assisted photoelectric conversion in the *c*-plane α-In_2Se_3 hexagonal microplate with SPV mode operation such as the band-bending diagram shown in the middle part of Figure 3c. In comparison with SPV, the SPR measurement needs the application of an external voltage V_0 in series with a load resistor R_L similar to PC. Nevertheless, an extra peak near 3.0 eV (denoted as SPR P2) appears in the SPR spectrum of Figure 3a. The energy position of SPR P1 also is lower than that of SPV P1 and close to that of PC P1. It means that the built-in electric fields for the three layers of In_2Se_3, $In_2Se_{3-3x}O_{3x}$, and In_2O_3 by SPR can be properly adjusted by changing V_0 to accommodate different photoresponse contributions from each of the three layers such as the band-bending diagram shown in the right side of Figure 3c. The photoresponse of the SPR P2 peak around 3 eV is inferred to come from the outermost layer of $\sim In_2O_3$.

To evaluate the different band-bending effects for the heterojunction layers of In_2Se_3-$In_2Se_{3-3x}O_{3x}$-In_2O_3 [see Figure 3c], bias-dependent SPR measurements were carried out at room temperature. Figure 4a shows the bias-dependent SPR spectra of α-In_2Se_3 with $V_0 = 20$ V (open-triangle line), $V_0 = 30$ V (open-circle line), and $V_0 = 40$ V (solid-triangle line), respectively. For the lower bias condition ($V_0 = 20$ V), the SPR P1 and SPR P2 peaks in the SPR spectrum of α-In_2Se_3 are smaller and are connected smoothly. The photoresponse contribution in this bias range mainly comes from both In_2Se_3 and $In_2Se_{3-3x}O_{3x}$ layers. Whereas when the bias increases to $V_0 = 30$ V, a clear feature near 3.0 eV is obviously detected. It is the SPR P2 peak contributed by the outermost layer of In_2O_3. With increased bias to $V_0 = 40$ V, both SPR P1 and SPR P2 and that of the connection spectrum from 1.8 to 3.2 eV are simultaneously enhanced. The photoresponsivities contributed from the $In_2Se_{3-3x}O_{3x}$ ($0 \le x \le 1$) layers show a dramatic increase. The surface oxide assisted photoelectric conversion in the different energy range from near-infrared to ultraviolet is controllable by a different surface band bending effect evident in Figure 4a. The surface oxide $In_2Se_{3-3x}O_{3x}$ ($0 \le x \le 1$) plays a key role for optical-electric conversion of the *c*-plane α-In_2Se_3. To further verify the existence of the surface oxide layer on the crystal plane of α-In_2Se_3, PL measurements at 20 and 300 K are respectively carried out. Displayed in Figure 4b are the PL spectra of the *c*-plane α-In_2Se_3. It is clearly that only one broadened peak centered at ~2.63 eV at 300 K is found. The emission is contributed by the $In_2Se_{3-3x}O_{3x}$ ($0 \le x \le 1$) surface oxide. When the temperature lowered down to 20 K, the PL peak shows an energy increase and a line-width (L_W) narrowing effect such as the general semiconductor behavior. The energy of the PL peak at 20 K is about 2.72 eV. The PL results of Figure 4b sustain that the adsorption of oxygen by Se vacancies in α-In_2Se_3 will form an oxidation layer $In_2Se_{3-3x}O_{3x}$ ($0 \le x \le$

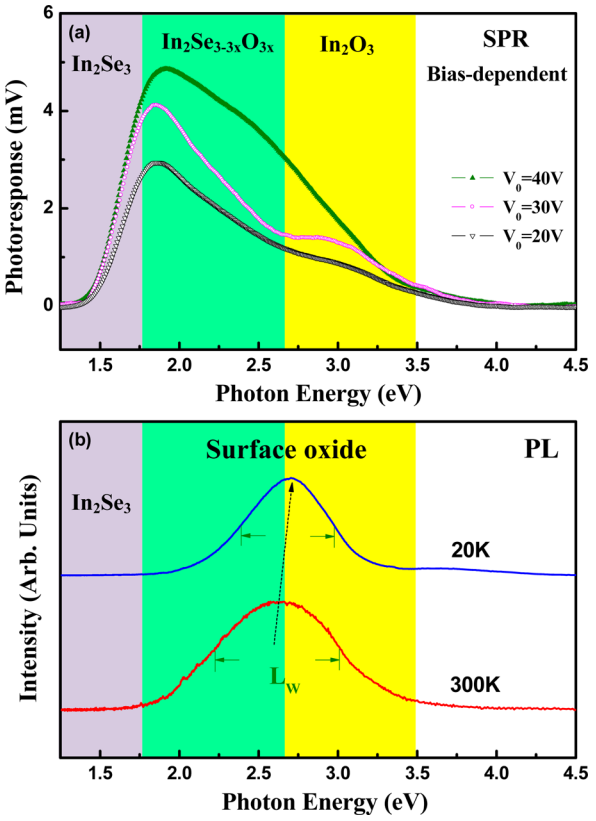

Figure 4. (a) Bias dependent SPR spectra of α-In_2Se_3 for showing different photoresponsivities from the oxide layers on the In_2Se_3-$In_2Se_{3-3x}O_{3x}$-In_2O_3 heterojunction structure. (b) The PL spectra of α-In_2Se_3 at 20 and 300 K showing that the PL emission peaks are coming from the surface oxide layer.

1). Because the formation of surface oxide layer, the PL signal from the inner α-In_2Se_3 bulk cannot strongly emit out.

Figure 5a displays the room-temperature TR and transmittance spectra of the *c*-plane α-In_2Se_3 in the energy range of 1.25 to 2 eV. The dashed line is the experimental TR spectrum and the open-circle line is the least-squares fit to a derivative Lorentzian line-shape function expressed as $\Delta R/R = \mathrm{Re}[\sum A \cdot e^{j\varphi}(E - E_g^d + j\Gamma)^{-m}]$,[35] where A and φ are the amplitude and phase of the line shape, and E_g^d and Γ are the energy and broadening parameters of the interband transition. The value of $m = 0.5$ is used for the first derivative line shape analysis of the critical-point transition of the direct band gap for α-In_2Se_3.[35] The obtained direct band gap of α-In_2Se_3 (indicated by arrow) is $E_g^d = 1.453$ eV at 300 K. The value of E_g^d is approximately in accordance with the center location of the transmittance spectrum for matching the absorption edge of α-In_2Se_3 as indicated in Figure 5a. It lends clear evidence that the α-In_2Se_3 hexagonal microplate is a direct semiconductor with its gap value in the near-infrared region. To further verify the E_g^d transition is responsible for the direct band gap of α-In_2Se_3, temperature-dependent TR measurements were carried out in the temperature range between 30 and 300 K. Figure 5b shows the temperature-dependent TR spectra of α-In_2Se_3 (dashed lines) in the energy range of 1.25−2 eV. The solid lines are those of the Lorentzian line-shape fits. The obtained energies of E_g^d show an energy-reduction behavior with the increase of temperatures from 30 to 300 K such as the general semiconductor behavior. The temperature dependence of transition energies of E_g^d from 30 to 300 K with representative

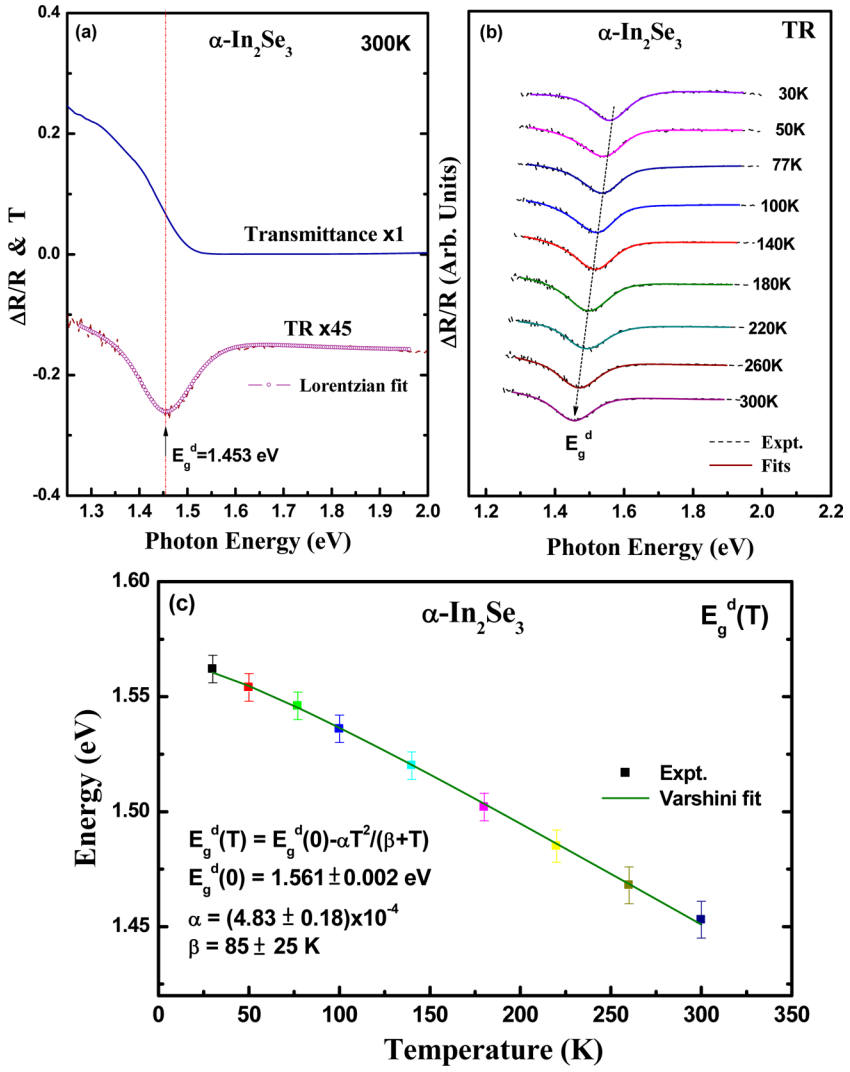

Figure 5. (a) Transmittance and TR spectra of α-In_2Se_3 for the identification of direct band gap. (b) Temperature-dependent TR spectra of α-In_2Se_3 from 30 to 300 K. (c) Temperature dependence of direct band gaps of α-In_2Se_3 between 30 and 300 K. The solid line is the least-squares fit of the experimental data using the Varshni equation.

error bar is depicted in Figure 5c. The solid line is the least-squares fit of the experimental data using the Varshni equation $E_g^d(T) = E_g^d(0) - \alpha \cdot T^2/(\beta + T)$, where $E_g^d(0)$ is the energy at 0 K, and α and β are constants referred to as the Varshni coefficients. The constant α is related to the electron−phonon interaction, and β is closely related to the Debye temperature. The obtained values of fitting parameters from Figure 5c are $E_g^d(0) = 1.561 \pm 0.002$ eV, $\alpha = (4.83 \pm 0.18) \times 10^{-4}$ eV/K, and $\beta = 85 \pm 25$ K, respectively. The obtained relationship of the temperature-dependent direct band gaps of α-In_2Se_3 can be utilized for α-In_2Se_3 when the material operated under sunlight above room temperature.

As shown in Figure 3a, the PC mode operation of the α-In_2Se_3 hexagonal microplate dominates the near-infrared to visible region while the SPR mode operation handles the detection in the visible to ultraviolet range. Specially, the bias-dependent SPR mode can properly adjust the detection wavelength region coming from the surface oxide layer α-$In_2Se_{3-3x}O_{3x}$ $(0 \le x \le 1)$ as evident in Figure 4a. Based on the experimental understanding of physical and chemical properties of α-In_2Se_3, a wide-energy-range and high-sensitivity photodetector that combines the PC and SPR mode operations for α-In_2Se_3 has been proposed and fabricated. A representative circuit scheme of the photodetector is depicted in Figure 6a. A switch SW1 selects the PC or SPR mode operation, and four resistors (R1−R4) set different bias conditions for the α-In_2Se_3 microplate. A buffer and an amplifier designated as the OP 37 operational amplifier are used for sensing photoelectric conversion signals from the α-In_2Se_3 microplates. Figure 6b demonstrates the testing functional performance of the PC and SPR mode photodetector made by α-In_2Se_3. The light source is a tungsten halogen lamp dispersed by a monochromator. The PC mode operation shows a high signal-to-noise ratio (SNR) response with a peak photosensitivity near 1.5 eV while when it selects the SPR mode, a well-behaved SNR photoresponse ranging from ∼1.5 to ∼3.8 eV can be detected. The results show that a wide energy range photodetector with detection ability from near-infrared to ultraviolet can be fabricated by using only one material (i.e., α-In_2Se_3) with different mode operations. Besides, as shown in the PC mode spectrum of Figure 6b, the optical absorption below the direct band gap (<1.453 eV) still shows higher photoresponse. It lends evidence that a defect-related optical absorption still occurred inside the α-In_2Se_3 material. This result facilitates the extension of the

dx.doi.org/10.1021/am400128e | ACS Appl. Mater. Interfaces 2013, 5, 2269−2277

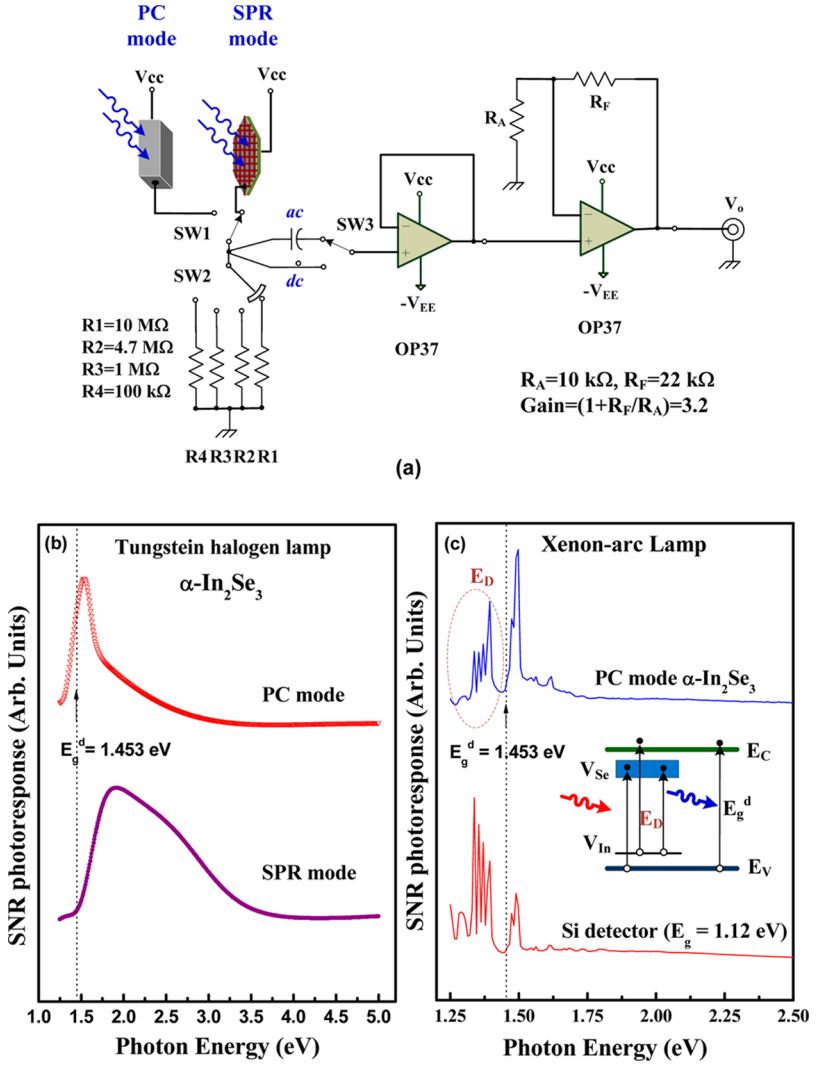

Figure 6. (a) Circuit design of PC and SPR mode photodetector for α-In_2Se_3. (b) The testing signal-to-noise ratio responses for PC mode and SPR mode operations in the energy range of 1.25−5 eV using a tungsten halogen lamp. (c) The PC mode photodetection of sharp line features in α-In_2Se_3 using xenon-arc lamp. The tested detector response for a commercialized Si photodiode is also included for comparison.

photoelectric conversion range of α-In_2Se_3 to a much longer wavelength region. Figure 6c shows the testing functional performance of the PC mode photodetector of α-In_2Se_3. The light source is a xenon-arc lamp which originally contains many plasma line features below 2 eV [see Figure 6c]. For comparison purpose, a commercialized silicon photodetector is also tested and compared. The value of the band gap of Si is 1.12 eV, lower than that of 1.453 eV for α-In_2Se_3. However, many sharp line features (E_D) below 1.453 eV can still be detected by the PC mode photodetector owing to the assistance of the defect transitions inside the α-In_2Se_3. In_2Se_3 is a naturally defect semiconductor comprising many of the Se vacancies (V_{Se}) and In vacancies (V_{In}) in the unit cell. It is similar to In_2S_3.[36] The V_{Se} may be the donor level, but V_{In} is an acceptor. The inset in Figure 6c depicts the representative band scheme below the band edge of α-In_2Se_3. The defect transitions (E_D) assist photoelectric conversion in the infrared region for In_2Se_3 as evident in the PC mode spectrum of Figure 6c. The PC mode α-In_2Se_3 also reveals larger photoresponsiveness than that of the Si detector with the energy higher than 1.45 eV [see Figure 6c]. All the testing results in Figures 6a, 6b, and 6c demonstrate that α-In_2Se_3 microplate is a photosensitive solar-energy material with surface formation oxide α-$In_2Se_{3-3x}O_{3x}$ ($0 \le x \le 1$) that assists the photoelectric conversion in the visible to ultraviolet region, while the bulk In_2Se_3 and defect transitions facilitate the optical absorption in the visible to infrared range.

CONCLUSION

Surface oxide assisted photoelectric conversion in α-In_2Se_3 hexagonal microplates has been first evaluated. Owing to the misvalency of III and VI atoms, α-In_2Se_3 microplate can form easily a surface oxidation layer α-$In_2Se_{3-3x}O_{3x}$ ($0 \le x \le 1$) on its crystalline face while it still contains many Se and In vacancies inside the bulk In_2Se_3. The existence of a surface oxide layer on α-In_2Se_3 was probed and verified by XPS, SPV, SPR, and PL measurements. The experimental results of SPV and SPR clearly show that the surface oxidation layer on α-In_2Se_3 assists photoelectric conversion in the visible to ultraviolet region. The detection range is extended far beyond the bulk α-In_2Se_3 with a direct gap of 1.453 eV. However, from the PC measurements of α-In_2Se_3, the bulk α-In_2Se_3 and V_{Se} and V_{In} vacancies sustain the photoelectric conversion of sunlight in the near-infrared to visible range. A simple junction

solar-cell structure like a SPV configuration proves that a maximum quantum efficiency of a copper-In_2O_3-$In_2Se_{3-3x}O_{3x}$-In_2Se_3 configuration is $\eta \approx 4.36\%$ close to the peak photoresponse near 2.18 eV. The value is close to the green portion near the maximum responsiveness of sunlight on earth. By integrating the PC and SPR mode operations of α-In_2Se_3, a photodetector with high sensitivity and wide spectral range from infrared to ultraviolet can be implemented. Both chemical and physical characteristics of the α-In_2Se_3 hexagonal microplate show that α-In_2Se_3 is a native solar energy material with well-behaved function operating under sunlight from near-infrared to ultraviolet.

AUTHOR INFORMATION

Corresponding Author

*Phone: +886 2 27303772. Fax: +886 2 27303733. E-mail: chho@mail.ntust.edu.tw.

Notes

The authors declare no competing financial interest.

ACKNOWLEDGMENTS

This work was sponsored by the National Science Council of Taiwan, Republic of China, under the Grant NSC101-2221-E-011-052-MY3.

REFERENCES

(1) Peng, H.; Schoen, D. T.; Meister, S.; Zhang, X. F.; Cui, Y. *J. Am. Chem. Soc.* **2007**, *129*, 34−35.
(2) Kwon, S. H.; Ahn, B. T.; Kim, S. K.; Yoon, K. H.; Song, J. *Thin Solid Films* **1998**, *323*, 265−269.
(3) Zhai, T.; Ma, Y.; Li, L.; Fang, X.; Liao, M.; Koide, Y.; Yao, J.; Bando, Y.; Golberg, D. *J. Mater. Chem.* **2012**, *20*, 6630−6637.
(4) Mitzi, B.; Copel, M.; Chey, S. J. *Adv. Mater.* **2005**, *17*, 1285−1289.
(5) Sreekumar, R.; Jayakrishnan, R.; Kartha, C. S.; Vijayakumar, K. P. *J. Appl. Phys.* **2006**, *100*, 033707.
(6) Lai, K.; Peng, H.; Kundhikanjana, W.; Schoen, D. T.; Xie, C.; Meister, S.; Cui, Y.; Kelly, M. A.; Shen, Z. X. *Nano Lett.* **2009**, *9*, 1265−1269.
(7) Lee, J. Y.; Sun, K.; Li, B.; Xie, Y. H.; Wei, X.; Russell, T. P. *Appl. Phys. Lett.* **2010**, *97*, 092114.
(8) Peng, H.; Xie, C.; Schoen, D. T.; Cui, Y. *Nano Lett.* **2008**, *8*, 1511−1516.
(9) Sreekmar, R.; Jayakrishnan, R.; Kartha, S. K.; Vijayakumar, K. P.; Khan, S. A.; Avasthi, D. K. *J. Appl. Phys.* **2008**, *103*, 023709.
(10) Li, Q. L.; Gao, L. J.; Wang, S. D.; Sun, X. H. *Appl. Phys. Lett.* **2011**, *99*, 243105.
(11) Zhai, T.; Fang, X.; Liao, M.; Xu, X.; Li, L.; Liu, B.; Koide, Y.; Ma, Y.; Yao, J.; Bando, Y.; Golberg, D. *ACS Nano* **2010**, *4*, 1596−1602.
(12) Whittingan, M. S. *Prog. Solid State Chem.* **1978**, *12*, 41−99.
(13) Merle, J. C.; Batiromo, R.; Borsella, E.; Piacentini, M.; Savoia, A. *Solid State Commun.* **1978**, *28*, 251−255.
(14) Hogg, J. H. C. *Acta Crystallogr.* **1971**, *B27*, 1630−1634.
(15) Li, Y.; Gao, J.; Li, Q.; Peng, M.; Sun, X.; Li, Y.; Yuan, G.; Wen, W.; Meyyappan, M. *J. Mater. Chem.* **2011**, *21*, 6944−6947.
(16) Ishikawa, M.; Nakayama, T. *Jpn. J. Appl. Phys.* **1998**, *37*, L1122−L1124.
(17) Ishikawa, M.; Nakayama, T. *Jpn. J. Appl. Phys.* **1997**, *36*, L1576−L1579.
(18) Marsillac, S.; Combot-Marie, A. M.; Bernéde, J. C.; Conan, A. *Thin Solid Films* **1996**, *288*, 14−20.
(19) Ye, J.; Soeda, S.; Nakamura, Y.; Nittono, O. *Jpn. J. Appl. Phys.* **1998**, *37*, 4264−4271.
(20) Emziane, M.; Marsillac, S.; Bernéde, J. C. *Mater. Chem. Phys.* **2000**, *62*, 84−87.
(21) Jansinski, J.; Swider, W.; Washburn, J.; Liliental-Weber, Z.; Chaiken, A.; Nauka, K.; Gibson, G. A.; Yang, C. C. *Appl. Phys. Lett.* **2002**, *81*, 4356−4358.
(22) Robles, R.; Barreau, N.; Vega, A.; Marsillac, S.; Bernède, J. C.; Mokrani, A. *Opt. Mater.* **2005**, *27*, 647−653.
(23) Ho, C. H.; Wang, Y. P.; Chan, C. H.; Huang, Y. S.; Li, C. H. *J. Appl. Phys.* **2012**, *108*, 043518.
(24) Ho, C. H. *J. Cryst. Growth* **2010**, *312*, 2718−2723.
(25) Wang, Y. P.; Ho, C. H.; Huang, Y. S. *J. Phys. D: Appl. Phys.* **2010**, *43*, 415301.
(26) Ho, C. H.; Lee, H. W.; Cheng, Z. H. *Rev. Sci. Instrum.* **2004**, *75*, 1098−1102.
(27) Ho, C. H. *Appl. Phys. Lett.* **2010**, *96*, 061902.
(28) Hsin, C. L.; Lee, W. F.; Huang, C. T.; Huang, C. W.; Wu, W. W.; Chen, L. J. *Nano Lett.* **2011**, *11*, 4348−4351.
(29) Hsu, C. L.; Lu, Y. C. *Nanoscale* **2012**, *4*, 5710−5717.
(30) Faur, M.; Faur, M.; Jayne, D. T.; Goradia, M.; Goradia, C. *Sur. Interface Anal.* **1990**, *15*, 641−650.
(31) Cahen, D.; Ireland, P. J.; Kazmerski, L. L.; Thiel, F. A. *J. Appl. Phys.* **1985**, *57*, 4761−4771.
(32) Neison, A. J.; Gebhard, S.; Kazmerski, L. L.; Colavita, E.; Engelhardt, M.; Höchst, H. *Appl. Phys. Lett.* **1990**, *57*, 1428−1430.
(33) Ho, C. H.; Chan, C. H.; Tien, L. C.; Huang, Y. S. *J. Phys. Chem. C* **2011**, *115*, 25088−25096.
(34) Tahar, R. B. H.; Ban, T.; Ohya, Y.; Takahashi, Y. *J. Appl. Phys.* **1997**, *82*, 865−870.
(35) Aspnes, D. E. In *Handbook on Semiconductors*; Balkanski, M., Ed.; North Holland: Amsterdam, The Netherlands, 1980.
(36) Ho, C. H. *J. Mater. Chem.* **2011**, *21*, 10518−10524.